A&A 553, A48 (2013)
DOI: 10.1051/0004-6361/201220311

Astronomy & Astrophysics

Near-infrared variability in the star-forming region RCW 38⋆

M. Dörr[1], R. Chini[1,2], M. Haas[1], R. Lemke[1], and D. Nürnberger[1]

[1] Astronomisches Institut, Ruhr-Universität Bochum, Universitätsstraße 150, 44801 Bochum, Germany
e-mail: chini@astro.rub.de
[2] Instituto de Astronomía, Universidad Católica del Norte, Antofagasta, Chile

Received 30 August 2012 / Accepted 11 March 2013

ABSTRACT

Aims. We want to study the content of young stellar objects in the RCW 38 cluster by means of multi-epoch variability studies.
Methods. We performed a three-month near-infrared (NIR) monitoring campaign of the young cluster RCW 38 using the 80 cm IRIS telescope near Cerro Armazones, Chile. Variability data with a median sampling of 1 day was gathered for 1026 sources, while a total of 3433 sources in *JHK* could be studied in the co-added, deep images with a completeness limit of $K < 15$ mag.
Results. We find that 139 sources were identified as variable with amplitudes above 10% in *H* and *K*, and 47% of these variables have been classified as candidate young stars by previous X-ray and mid-infrared studies. Although the majority of the variable sources show no *K*-excess, their high extinction and concentration towards the cluster center, together with their irregular variability behavior, suggest that they are also candidate young stellar objects. Most of them are likely low-mass sources with variability amplitudes typical of T Tauri stars. The majority of previously suggested OB candidates appear to be intermediate-mass pre-main sequence sources on the basis of their *JHK* properties.
Conclusions. NIR variability is an efficient tool for detecting new, embedded, young stellar objects that have escaped previous X-ray and mid-infrared studies.

Key words. stars: formation – stars: pre-main sequence – stars: variables: T Tauri, Herbig Ae/Be – stars: early-type – stars: late-type – open clusters and associations: individual: RCW 38

1. Introduction

Although photometric variability is one of the classical characteristics of young stellar objects (YSOs; Joy 1945; Herbig 1962), apart from extensive monitoring campaigns of individual objects – particularly at optical wavelengths – this time-consuming technique has been rarely used in comprehensive wide-field studies during the past decades. Using the 2MASS south telescope, Carpenter et al. (2001, 2002) performed wide-field near infrared (NIR) variability studies of stars towards the Orion A and Chamaeleon I star-forming regions. More recently, Rice et al. (2012) have monitored the dark cloud L 1003 in Cygnus OB7 at NIR wavelengths with UKIRT over a time span of 1.5 years, and Morales et al. (2011, 2012) collected multi-epoch, multi-color light curves of candidate members of the Orion nebular cluster region during their dedicated Warm *Spitzer* Exploration Science Program YSOVAR (complemented by UKIRT and CFHT data). Likewise, a comprehensive long-term (meanwhile spanning 8 yrs) monitoring campaign of NIR variability in a large sample of brown dwarfs and T Tauri stars has been carried out by Scholz and collaborators (Scholz et al. 2009; Scholz 2012).

Variability is a valuable probe for both stellar and circumstellar activities. The causes for periodic variability are thought to originate in hot accretion or cool magnetic spots that rotate with the star, whereas aperiodic variability may arise from coronal flares, irregular accretion, and variations in circumstellar extinction. Observationally, variations are detected from X-ray to ultraviolet, infrared, and radio wavelengths, where each regime probes a different aspect of the YSO and its circumstellar environment (Bouvier & Bertout 1989). Near-infrared monitoring observations as described in the present paper are expected to probe those temperature, opacity, and geometry changes in the circumstellar environment that are not accessible to shorter wavelength studies.

RCW 38 is an area of high-mass star formation at a distance of 1.7 kpc; for an overview of early observations, we refer to a review by Wolk et al. (2006). The HII region is excited by the O5.5 binary RCW 38 IRS 2 (Frogel & Persson 1974; DeRose et al. 2009). DeRose et al. (2009) also identify 314 cluster members from a total of 336 *JHK* detections in a field of 56″ × 56″ around IRS 2. A similar number of cluster stars were previously inferred from Chandra observations, covering a field of view (FoV) of about 16′ × 16′; Wolk et al. (2006) associated 360 X-ray sources out of 460 detections with the star-forming region. Recently, Winston et al. (2011) have presented *Spitzer* observations from a 30′ × 30′ field and identified 624 YSOs on the basis of infrared photometry from 2MASS (1.2–2.2 μm) and IRAC (3–8 μm). Furthermore, they find 72 stars that exhibit IR variability.

Apart from the described low-mass population, Wolk et al. (2006) suggest the presence of 31 OB candidates in a field of ∼10′ × 10′, while Winston et al. (2011) even report identifying 27 further O and a total of 604 OB star candidates in a field of ∼30′ × 30′. Both studies used the extinction-corrected *K* band luminosity function to infer stellar types earlier than B9.

In this paper, we present a 40-epoch *JHK* monitoring study of RCW 38. Section 2 describes our data set and the reduction procedures. In Sect. 3, we identify the variable stars, and discuss

⋆ Full Tables 1 and 2 are only available at the CDS via anonymous ftp to cdsarc.u-strasbg.fr (130.79.128.5) or via http://cdsarc.u-strasbg.fr/viz-bin/qcat?J/A+A/553/A48

their properties in Sect. 4. Sources of special interest and cluster properties are discussed in the final Sect. 5.

2. Observations and data

2.1. Observations

Observations were carried out using the 80 cm IRIS telescope of the Universitätssternwarte Bochum near Cerro Armazones, Chile at an altitude of 2817 m. IRIS is equipped with IRISCAM, a 1024 × 1024 NIR detector array with a field of view of 12.5′ × 12.5′ and a resolution of 0.74″ per pixel. Thanks to their compatibility with the 2MASS color system, we chose J, H, and K_s (henceforth simply denoted as K) filters for this study. Further information about IRIS is given in Hodapp et al. (2010).

The monitoring campaign was scheduled from January to March 2011. However, the Bolivian winter prevented observations during the entire month of February. Other nights with bad observing conditions were rejected on-site, resulting in a total of 40 nights of K band data. If possible, observations in J and H were also performed. Typical integration times lie between three and five minutes per filter per night.

To avoid errors from inhomogeneous sky emission, a sky field 50′to the southeast was chosen. This close sky field also allowed fast object-sky/sky-object cycles below one minute, thus avoiding problems with temporal sky background variation.

2.2. Data reduction

Raw data were reduced for bias, dark, flat, and sky background emission using standard IRAF procedures, while astrometric correction was performed using SCAMP (Bertin 2006). All frames in one filter of a given night were combined, resulting in one image per night per filter. Because of both the high density of sources and strong nebular emission, IRAF *psf* photometry was performed on 1579 sources. Carefully selected, nonvariable stars with a mean photometric error of 0.02 mag in K were used as templates for the *psf* fitting routine. These stars were also selected to correct for transmission changes between the nights, thus adding a ∼2% systematic error.

In a second step, all images from one filter were co-added into one deep image, with photometry performed as before. Calibration was achieved by using the best (quality flag AAA) stars from the 2MASS catalog and checked for linearity. With the longer net integration time, the co-added data set contains 3433 sources with a histogram-determined K detection limit of ∼15 mag. Half of the sources show photometric errors ≤0.05 mag, while 23% show errors >0.1 mag and were excluded from the subsequent variability study. Nevertheless, attention has to be paid to bright sources with atypically high errors due to high background emission from the nebula.

2.3. Identification of variable stars

As discussed in Haas et al. (2012), purely statistical identification of variables can lead to different biases. Compared to using the standard deviation and amplitude of the light curves, the widely used J-Index (Stetson 1996) seems to be particularly sensitive for finding variables with small amplitudes among faint noisy stars in light curves with many (>50) data points. Because our light curves have only 40 data points, we restrict the variability search here to the amplitude method.

Therefore, selection of variable sources was handled in the following way. To avoid false detections due to high noise, fainter stars (K > 15 mag) were excluded. From these 1026 objects, only those with variability amplitudes larger than 10% in all three filters were considered as candidate variable stars. Because the J-band light curves exhibit higher noise, we are restricted to the H- and K-band light curves alone. As a final selection criterion, we picked out only those sources that displayed consistent variability patterns in H and K; of course, this procedure rejects possible sources with strong color variations. The described procedure yielded 139 stars as bona fide variable sources. Their position within RCW 38 and their variability amplitude are marked in Fig. 1. Details on these variables are listed in Table 1, while individual H and K measurements can be found in Table 2.

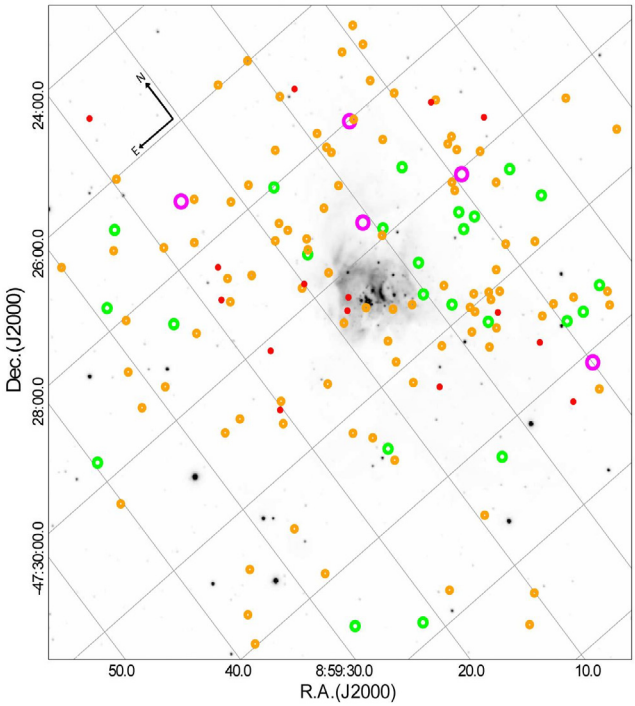

Fig. 1. K-image of RCW 38 co-added from 40 nights. The 139 variables identified in this work are encircled, and their variability amplitude is indicated by both color and symbol size. Amplitudes ≤0.2 mag are red, ≤0.5 mag orange, ≤1 mag green, and >1 mag magenta.

3. Results

3.1. Variability

Seventy-eight percent of the variable stars exhibit irregular light curves with typical timescales of a few days and amplitudes between 0.1 and 0.4 mag in K (Fig. 2a). A few of these sources show variations and outbursts with amplitudes above 1 mag (Fig. 2b). The light curves of 13% of stars have a low-amplitude periodic pattern on timescales of several days (Fig. 2c). Due to the lack of sufficient data, in-depth period fitting methods were not possible. Nine percent of the sources show a slow change in brightness, suggesting long-term variations (Fig. 2d).

3.2. Photometry of the co-added deep images

While co-added images lose the time variation information, their high integration time provides a much better signal-to-noise photometry and is thus ideal to obtain additional information on the

Table 1. Photometry of variable sources.

ID	RA (J2000)	Dec (J2000)	J (mag)	H (mag)	K (mag)	Ampl. (mag)	Var. behav.	MIR class.	Xray, MIR var.	cross-ID
23	08:59:30.00	−47:26:33.7	16.35 ± 0.02	15.18 ± 0.01	14.61 ± 0.04	0.3	i	II	X	202
52	08:59:17.88	−47:24:52.9	18.24 ± 0.06	15.65 ± 0.01	14.18 ± 0.03	0.3	i			
85	08:59:24.38	−47:26:57.6	17.47 ± 0.03	15.72 ± 0.01	14.70 ± 0.03	0.4	i	II		91
86	08:59:22.94	−47:26:41.4	17.89 ± 0.04	16.01 ± 0.02	14.72 ± 0.02	0.7	p			
164	08:59:15.31	−47:27:05.9	18.09 ± 0.06	15.43 ± 0.02	13.04 ± 0.01	3.0	i	0/I	X,v	291
227	08:59:16.39	−47:28:25.7	15.64 ± 0.01	13.78 ± 0.01	12.60 ± 0.01	0.2	l	FS		198

Notes. Variability behavior is denoted with "i" (irregular), "p" (periodic) and "l" (long term). Mid-infrared YSO classifications, X-ray detections, as well as cross-IDs from Winston et al. (2011; their Table 3) are given in the last three columns and denoted with 0/I, II, III (T Tauri classes), FS (flat-spectrum T Tauri), X (X-ray emission), and v (long-term MIR variation). For illustration, a few entries are displayed; the entire table is available at the CDS.

Table 2. Daily photometry for all variable sources.

ID	MJD	H (mag)	K (mag)
23	55 568.345	15.15 ± 0.02	14.70 ± 0.06
23	55 570.142		14.62 ± 0.03
23	55 572.111	15.15 ± 0.01	
23	55 573.212	15.18 ± 0.02	14.59 ± 0.02

Notes. For illustration a few lines are displayed; the full table is available at the CDS. The epochs (MJD) of a single night with both H and K observations differ by less than 2 h, so the average MJD is listed.

average properties of the variable sources; simultaneously they reveal fainter objects in the RCW 38 cluster.

Figure 3 shows the *JHK* color–color diagram for 977 stars with $K < 15$ mag and errors <0.15 mag. The main sequence was constructed from NIR colors from Ducati et al. (2001). The reddening paths correspond to $A_V = 30$ mag for a ratio of total-to-selective extinction of $R = 3.1$ (Rieke & Lebofsky 1985). The location of most of the stars close or below the upper reddening path corroborates the quality of our co-added photometry. In contrast, a similar plot of the corresponding 2MASS data yields a large scatter of locations all over the diagram.

Most sources are reddened by more than 10 mag. Sources thrice the maximum acceptable error for variables of 0.1 mag to the right of the lower reddening path are defined as IR-excess objects, thus indicating hot circumstellar material. Sixteen percent of the variables can be identified with this further tracer for youth.

The color–magnitude diagram in Fig. 4 shows all (3042) stars detected simultaneously at H and K. Obviously, the variables occur predominantly among the fainter stars: 91% have $H > 14$ mag and still 65% of the sources are fainter than $H = 15$ mag.

4. Nature of the variable stars

4.1. Association with the star-forming cloud

To evaluate the association of the detected variables with RCW 38 we have a closer look onto the line-of-sight extinction toward the region. The CO map from Gillespie et al. (1979) indicates a massive cloud with a diameter of ∼30′, i.e. larger than the field of view of our IR study. The 1 mm dust continuum data by Cheung et al. (1980) suggest high density within the central 5′ and a peak extinction of $A_V = 800$ mag. This excludes contamination by background sources in the center. Therefore, background contamination could occur only at the edges of our 11.37′ × 11.03′ field. Including all sources with amplitudes

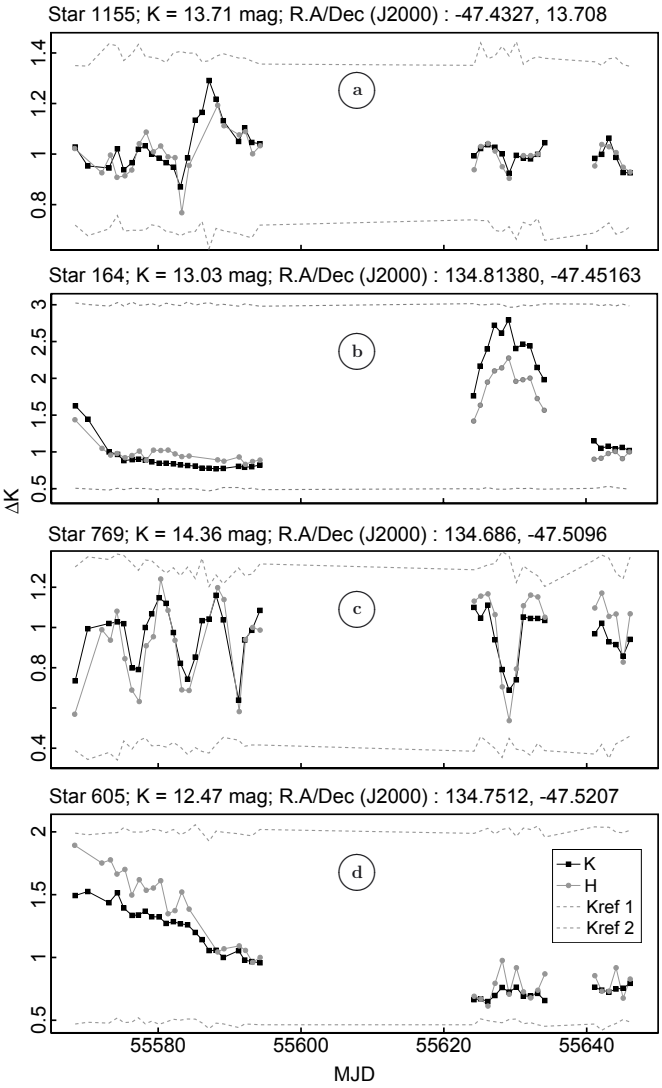

Fig. 2. Four typical light curves for variable stars (black dots K, gray dots H). The dashed lines represent two nearby nonvariable stars in K. *From top to bottom*, the individual panels show the following cases: **a)** Irregular variability, typical for most variable sources in this data set. **b)** Irregular variability with high amplitude and outburst. **c)** Candidate periodic star, representative of 13% of variables. **d)** Slow brightness change with possible periodic behavior, which can be found in 9% of variable sources.

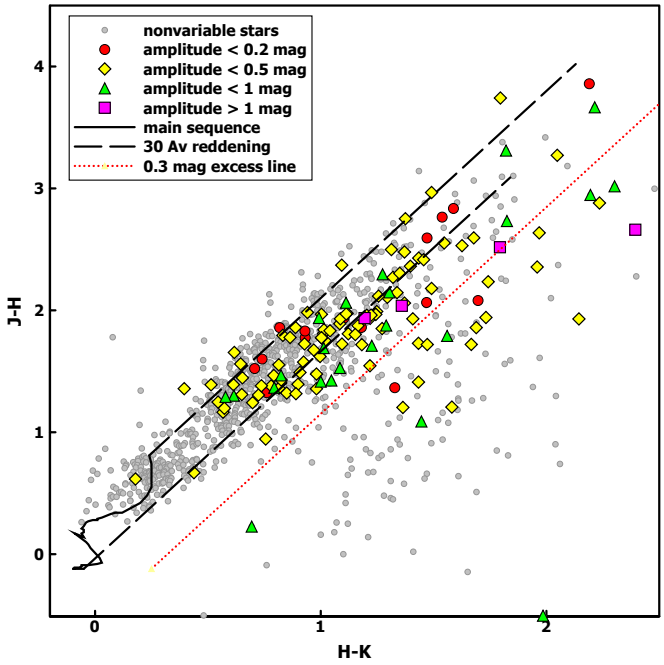

Fig. 3. *JHK* color–color diagram for 977 stars with $K < 15$ mag. Nonvariable sources with combined errors <0.15 mag are shown in gray, the 136 variable sources with complete *JHK* data sets have colored symbols. The color codes for the K-variability are the following: amplitudes ≤0.2 mag red, ≤0.5 mag yellow, ≤1 mag green, and >1 mag magenta. The curve denotes the main sequence from M4 to B0 (Ducati et al. 2001), the dashed lines correspond to reddening paths for $A_V = 30$ mag, and the dotted line marks the limit for K-excess sources.

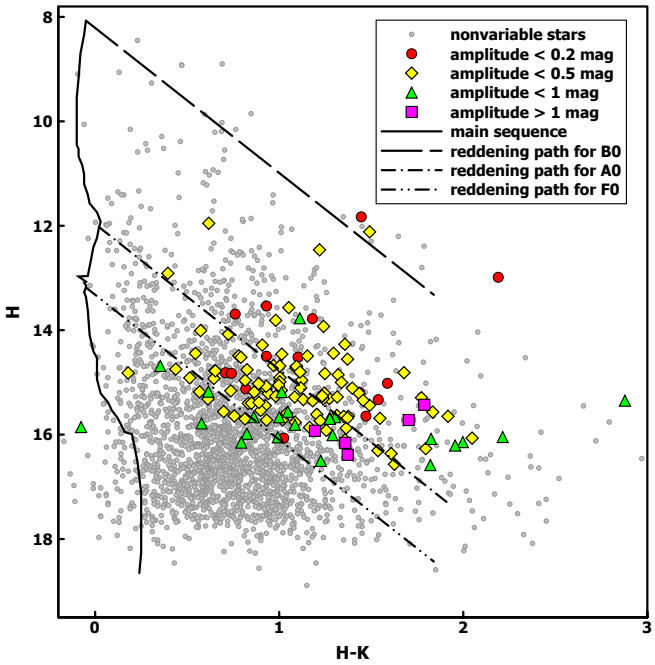

Fig. 4. H vs. $H - K$ color–magnitude diagram for 3042 stars toward RCW 38; same notation as Fig. 3. The main sequence (Ducati et al. 2001) was adapted to a distance of 1.7 kpc; the reddening paths (A_V = 30 mag) are drawn for spectral types B0, A0 and F0, respectively.

greater than 1 mag, 89% of variables can be found within a 5′ radius (~63% of entire FOV) around the central source, thus arguing in favor of an association with the cluster. Contamination by foreground sources can also be excluded because most variables have a mean A_V of ~15 mag (see Fig. 4). This corroborates our suggestion that the vast majority of variable sources are cluster members. The lack of detections toward the bright nebula is due to the high – and spatially variable – nebular emission, rendering stellar variability detection difficult.

4.2. Spectral types

The H vs. $H - K$ color–magnitude diagram can be used to estimate stellar spectral types. However, before shifting the stars back along the reddening path onto the main sequence, we correct for the IR-excess as determined from the *JHK* diagram. Here, we adopt the IR-excess to originate primarily in the K-band, thus offsetting the source only towards higher $H-K$ values. After applying the corresponding K-excess correction, the majority of variable sources (67%) lie below the reddening line for main sequence A-type stars, and only 12% of sources can be found above the reddening line for a B3 star.

Most variables are suspected of being pre-main sequence stars on their way to the main sequence, with higher luminosities and/or redder colors than a main-sequence star of similar mass. Therefore, the stars classified as A to F types will probably have later spectral types (i.e., lower masses) when on the main sequence, consistent with their typical T Tauri type variability.

4.3. Variability timescales and amplitude

Most variable sources in our sample display irregular variability with low amplitudes as illustrated in Fig. 2a. This is consistent with the nonperiodic, hot-spot driven variations found in accreting classical T Tauri stars. Periodic sources like the one in Fig. 2c with periods on timescales of several days and small amplitudes fit the behavior of one or more rotating cool spots or a relatively stable hot spot on a young star, with typical rotation periods between two and eight days (Eaton et al. 1995). The error bars should also allow for a classical Cepheid with a more sawtooth-like light curve. However, Cepheids are too old for this young cluster and would therefore have to be located in the background. A good reference for typical T Tauri variability patterns is given in Herbst et al. (1994).

Forty-seven percent of our variable sources have already been identified as candidate YSOs by previous studies using X-ray or mid-infrared (MIR) emission (Wolk et al. 2006; Winston et al. 2011), corroborating the potential of identifying YSOs via their variability. On the other hand, we suggest that the majority of the remaining 53% of variable sources are also YSO candidates that have escaped detection by classical methods.

5. Objects of special interest

5.1. OB star candidates

The central O5 binary IRS 2 (DeRose et al. 2009) can basically account for the observed radio flux (Goss & Shaver 1970; Furniss et al. 1975), leaving little to no room for further high-mass stars that contribute to the excitation of the nebula. Nevertheless, Wolk et al. (2006) find an additional 31 candidate OB stars (spectral type earlier than B9) within our field of view, based on *JHK* data and using the extinction-corrected K luminosity function. Obviously, pre-main sequence stars and/or circumstellar dust emission (K-excess) may simulate a K-brightness that is several magnitudes higher than the corresponding main sequence brightness. Our data set contains 27 of these OB candidates, of which five objects are classified

as O-type stars – according to their NIR colors. Twenty of them can be identified as YSOs based on MIR excess (Winston et al. 2011). Three of the suggested O-type candidates display K-excess in our data. The presence of circumstellar dust almost excludes the possibility that these objects are O-type stars. Furthermore, there are four sources that show variability in H and K: one of them is a suggested O-type candidate, and two other objects vary at MIR wavelengths. We therefore suggest that the majority of proposed OB candidates are fairly late B-type stars or even stars with lower mass.

5.2. IR-excess candidates

Despite our short monitoring campaign and strict variability criteria, 19% of K-excess candidates show NIR variability (i.e., 23 out of 120; one source with $H - K = 3.36$ mag and $J - H = 5.07$ mag is located outside of the plot range of Fig. 3). This suggests that the true number of K-excess sources associated with NIR variability might be (significantly) higher than the lower limit found in our study. Within our field of view, Winston et al. (2011) find 281 MIR excess sources using *Spitzer* and 2MASS data, out of which 17 show K-excess in our IRIS data. While *Spitzer* is more suited to finding excess sources, our photometry from the deep maps (~3 h integration time) reaches higher precision than 2MASS, enabling us to find 57 new candidate excess sources.

6. Summary and conclusion

On the basis of a 40-epoch *JHK* monitoring campaign spread over three months, we have almost doubled the number of variable sources in the star-forming region RCW 38. Only a third of these 79 new variables show K-excess as direct evidence of their youth. Nevertheless, due to their concentration towards the cluster center, high extinction, and irregular variability, we suggest that all NIR variables are candidate YSOs, too. Most of the variability amplitudes are above 10% in H and K, which is typical of T Tauri stars. The absence of K-excess in many sources is probably due to an eroded inner part of the circumstellar disk.

As a by-product of our study, we found K-excess for three sources and NIR variability for one source that have been classified as O-type candidates previously. We argued that the presence of circumstellar dust almost excludes the possibility of these sources being O-type stars, and suggested their reclassification as intermediate-mass pre-main sequence sources.

Our study has shown that NIR variability is a sensitive and efficient tool for detecting new, embedded, young stellar objects that have escaped previous X-ray and MIR surveys.

Acknowledgements. We thank the anonymous referee for constructive and helpful feedback. This work was supported by Nordrhein-Westfälische Akademie der Wissenschaften und der Künste.

References

Bertin, E. 2006, Astronomical Data Analysis Software and Systems XV, 351, 112
Bouvier, J., & Bertout, C. 1989, A&A, 211, 99
Carpenter, J. M., Hillenbrand, L. A., & Skrutskie, M. F. 2001, AJ, 121, 3160
Carpenter, J. M., Hillenbrand, L. A., Skrutskie, M. F., & Meyer, M. R. 2002, AJ, 124, 1001
Cheung, L. H., Frogel, J. A., Hauser, M. G., & Gezari, D. Y. 1980, ApJ, 240, 74
DeRose, K. L., Bourke, T. L., Gutermuth, R. A., et al. 2009, AJ, 138, 33
Ducati, J. R., Bevilacqua, C. M., Rembold, S. B., & Ribeiro, D. 2001, ApJ, 558, 309
Eaton, N. L., Herbst, W., & Hillenbrand, L. A. 1995, AJ, 110, 1735
Frogel, J. A., & Persson, S. E. 1974, ApJ, 192, 351
Furniss, I., Jennings, R. E., & Moorwood, A. F. M. 1975, ApJ, 202, 400
Gillespie, A. R., White, G. J., & Watt, G. D. 1979, MNRAS, 186, 383
Goss, W. M., & Shaver, P. A. 1970, Australian J. Phys. Astrophys. Supp., 14, 1
Haas, M., Hackstein, M., Ramolla, M., et al. 2012, Astron. Nachr., 333, 706
Herbig, G. H. 1962, Ad. Astron. Astrophys., 1, 47
Herbst, W., Herbst, D. K., Grossman, E. J., & Weinstein, D. 1994, AJ, 108, 1906
Hodapp, K. W., Chini, R., Reipurth, B., et al. 2010, Proc. SPIE, 7735
Joy, A. H. 1945, ApJ, 102, 168
Morales-Calderón, M., Stauffer, J. R., Hillenbrand, L. A., et al. 2011, ApJ, 733, 50
Morales-Calderón, M., Stauffer, J. R., Stassun, K. G., et al. 2012, ApJ, 753, 149
Rice, T. S., Wolk, S. J., & Aspin, C. 2012, ApJ, 755, 65
Rieke, G. H., & Lebofsky, M. J. 1985, ApJ, 288, 618
Scholz, A. 2012, MNRAS, 420, 1495
Scholz, A., Xu, X., Jayawardhana, R., et al. 2009, MNRAS, 398, 873
Stetson, P. B. 1996, PASP, 108, 851
Winston, E., Wolk, S. J., Bourke, T. L., et al. 2011, ApJ, 743, 166
Wolk, S. J., Spitzbart, B. D., Bourke, T. L., & Alves, J. 2006, AJ, 132, 1100